Critical properties of loop percolation models with optimization constraints

Frank O. Pfeiffer and Heiko Rieger
Theoretische Physik, Universität des Saarlandes, 66041 Saarbrücken, Germany
(Received 20 December 2002; published 19 May 2003)

We study loop percolation models in two and in three space dimensions, in which configurations of occupied bonds are forced to form a closed loop. We show that the uncorrelated occupation of elementary plaquettes of the square and the simple cubic lattice by elementary loops leads to a percolation transition that is in the same universality class as the conventional percolation. In contrast to this, an optimization constraint for the loop configurations, which then have to minimize a particular generic energy function, leads to a percolation transition that constitutes a universality class for which we report the critical exponents. Implication for the physics of solid-on-solid and vortex glass models are discussed.

DOI: 10.1103/PhysRevE.67.056113 PACS number(s): 64.60.Ak, 64.60.Cn, 64.60.Fr

I. INTRODUCTION

The percolation of loops (or closed strings) appears naturally in the context of liquid helium [1,2], early universe [3,4], high-temperature superconductors [5,6], and elastic media [7–9], where loops represent world lines, cosmic strings, vortex loops and height contour loops, respectively. In analogy to the characteristic size of a cluster in conventional site or bond percolation [10], the typical diameter ξ of the loops diverges when approaching a critical point, the loop percolation transition. This transition shows power-law behavior at the critical point, which is described by a set of critical exponents that constitute a universality class.

The elastic medium in two dimensions (2D) and amorphous high-T_c superconductors in 3D can be described by the solid-on-solid (SOS) model [9] and the vortex glass model [5,11], respectively, where the loop configurations are obtained from the optimization of an energetic cost function subject to a divergence (or loop) constraint. Recently, we analyzed [6] the loop statistics of vortex glass model and found an unconventional percolation transition of vortex loops in the ground state as a function of the disorder strength σ. A similar study in two dimensions, which is relevant to a disorder-driven transition in the SOS model, has not been performed yet.

In this paper we study these percolation transitions, numerically. We show that an optimization constraint for the loop configurations, which have to minimize a particular generic energy function, plays the key role for an unconventional percolation transition of vortex loops in the ground state as a function of the disorder strength σ. Therefore, we study two models with and without an optimization constraint. The *loop percolation* (LP) model without an optimization, in which each elementary plaquette of a square lattice (in 2D) or on a simple cubic lattice (in 3D) is occupied with a probability p with an elementary loop, is shown to be in the same universality as the conventional d-dimensional percolation. In contrast to the LP model, the *loop Hamiltonian* (LH) model with an optimization leads to a percolation transition that constitutes a new universality class, for which we report the critical exponents. For simplicity we choose uniform probability distributions for the disorder variables in the LH model, which slightly differ from distributions used for the SOS model [9,12,13] and the vortex glass model [11,6]. We show that this difference does not affect the universality.

The paper is organized as follows. In Sec. II, we introduce the models and the definition of *loops* (clusters). We describe the mapping of our models to the SOS model and the vortex glass model. In Sec. III we locate the percolation transition in each model and calculate the critical exponents using finite-size scaling (FSS). Section IV concludes the paper with a summary and a discussion.

II. MODELS

Consider a d-dimensional hypercubic lattice—i.e., a square lattice in 2D or a simple cubic lattice in 3D—of linear size L ($L=7$ in the 2D example in Fig. 1) with free boundary conditions. In the LP model the elementary plaquettes of the lattice are occupied by elementary loops with a probability p_1. [There are $(L-1)^2$ elementary plaquettes in 2D and $3L(L-1)^2$ elementary plaquettes in 3D.] An elementary loop consists of the four bonds belonging to an elementary plaquette plus a randomly chosen direction: either clockwise or counterclockwise, both with probability 1/2 (see Fig. 1). When two adjacent plaquettes are occupied by elementary loops of same orientation we cancel the occupation of the common bond as indicated in Fig. 1.

We can identify the resulting (directed) bond configuration of the LP model with a flow $\mathbf{n}=\{n_1,n_2,\ldots,n_M\}$, where n_i is an integer and M is the number of bonds in the lattice. We say that $n_i=0$ if bond i is not occupied, $n_i=\pm 1$ if it is singly occupied in the positive (negative) direction (positive and negative are defined by the introduction of an appropriate coordinate system), $n_i=\pm 2$ if it is doubly occupied, etc. Thus, an elementary loop (e.g., in the xy plane) can be represented by $n_{x,y}=n_{x+1,y}=-n_{x+1,y+1}=-n_{x,y+1}=1$ if oriented counterclockwise, as shown in Fig. 1. The complete flow $\mathbf{n}$ then can simply be thought of as the sum of all elementary loops. Obviously, in this sum the flow variables on the common bonds of adjacent elementary loops cancel arithmetically. Moreover, the construction of this flow via addition of elementary loops implies that on each site of the lattice the number of ingoing arrows balances the number

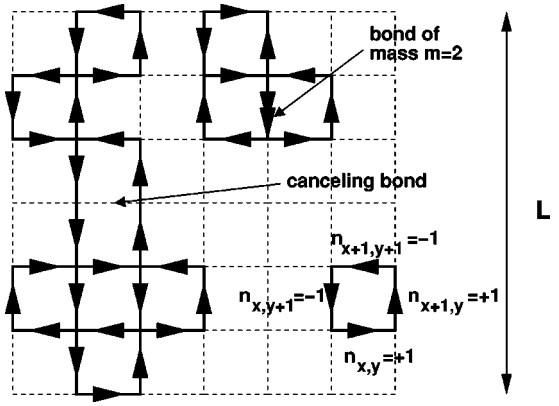

FIG. 1. Configuration **n** of the loop percolation model on a two-dimensional square lattice with system size $L=7$.

of outgoing arrows (see Fig. 1): one says that this flow is divergence free,

$$\nabla n_i = 0. \tag{1}$$

(The lattice-divergence operator is defined on each lattice site and sums simply all two-dimensional flow variables of the bonds connected to it.)

In analogy to conventional bond percolation we are now going to define the clusters of a configuration of the LP model: Two occupied bonds belong to the same cluster if they have one site in common. Thus, all bonds of the cluster can be connected via a directed path along occupied bonds belonging to this cluster, which is analogous to conventional bond percolation—up to the attribute *directed*. This is actually a slightly nontrivial observation—see Fig. 1 to exemplify this statement—because an occupied directed bond cannot be traversed in the opposite direction, but is a direct consequence of the fact that a cluster is also a sum of elementary loops.

The mass m of a cluster is the number of occupied bonds, where a bond i with a flow n_i counts $|n_i|$ times, i.e., has mass $m_i=|n_i|$. A percolating cluster is a cluster spanning the entire system (in at least one of the d directions). This implies that the cluster contains a directed path along its occupied bonds from one side of the lattice to the opposite. In the following we refer to the cluster just defined as a loop.

The representation of the configuration of directed occupied bonds as a flow **n** is now used to define the LP model *with* an optimization constraint: In contrast to the stochastic *uncorrelated* occupation of elementary loops in the LP model above, we now consider a different type of occupation of loops, which results from the minimization of an energy function for a loop configuration **n**,

$$H=H\{\mathbf{n}\}=\sum_{i=1}^{M} f_i(n_i), \tag{2}$$

where the sum is over all bonds i on a d-dimensional hypercubic L^d lattice with periodic boundary conditions. Herewith, we assume the energy function to be composed solely of local terms $f_i(n)$ with $f_i(n)\geqslant 0$ and convex [i.e., $f''(n)\geqslant 0$] for all bonds i and flow (or occupation) values n. Such energy functions are relevant in the context of disordered solid-on-solid models (in 2D) [9,12,13] and vortex glasses (in 3D) [11] since they determine their ground states. One has to keep in mind that the loop condition (1) has to be fulfilled—i.e., the optimization task consists in finding the minimum of Eq. (2) under the constraint (1).

For $f_i(n)=f(n)$ independent of the bond index the minimum is trivial: $n=0$, i.e., no bond is occupied. Only if the minima of local cost functions vary from bond index to bond index in a nontrivial way, one can expect a nontrivial loop configuration. We assume a random distribution of these minima (at values b_i) and restrict ourselves to a quadratic form of $f_i(n)$ around these minima: $f_i(n_i)=(n_i-b_i)^2$, which means that we study the loop configurations [i.e., occupied bond configurations that fulfill Eq. (1)] that minimize

$$H=\sum_i (n_i-b_i)^2. \tag{3}$$

The random variables b_i are uniformly distributed $b_i \in[-2\sigma,2\sigma]$ at a fixed *disorder strength* $\sigma\in[0,1]$. Here, the probability p to occupy a bond depends on the disorder strength σ. We refer to the LP model *with* an optimization constraint of Hamiltonian (3) as the *loop Hamiltonian* model. For the minimization of a free energy (optimization) we restrict to the calculation of the ground state $(T=0)$ configuration **n**, which is a minimum cost flow problem that can be solved *exactly* in polynomial time with appropriate algorithms [14].

The physical motivation of studying models like Eq. (3) under constraint (1) is the following: In 2D, Hamiltonian (3) occurs, for instance, in the context of the SOS model on a disordered substrate [7–9]. The SOS representation of a 2D surface is defined by integer height variables $u_k\in$ IN for each lattice site k of a square lattice. The disordered substrate is modeled via random offsets $d_k\in[0,1]$ for each lattice site, such that the total height at lattice site n is $h_k=u_k+d_k$. The total energy of the surface is

$$H_{\mathrm{SOS}}=\sum_{\langle k,l\rangle}(h_k-h_l)^2=\sum_{\langle k,l\rangle}(n_{kl}-b_{kl})^2, \tag{4}$$

where the sum runs over all nearest neighbor pairs of the square lattice and we introduced the height differences $n_{kl}=u_k-u_l$ and the offset differences $b_{kl}=d_k-d_l$, which both live on the bonds rather than then the sites of the lattice. The SOS Hamiltonian (4) is identical with Eq. (3) and as per definition the variables n_{kl} satisfy constraint (1). Therefore the SOS model on a disordered substrate is a physical representation of the LH model in 2D that we study here.

In 3D, Hamiltonian (3) is the strong screening limit of the vortex glass model for disordered superconductors [11,15,16],

$$H_{\mathrm{VG}}=\sum_{i,j}(n_i-b_i)G_\lambda(\mathbf{r}_i-\mathbf{r}_j)(n_j-b_j), \tag{5}$$

where the integer vortex variables $n_i\in$ IN live in the bonds of a simple cubic lattice and have to fulfill constraint (1)

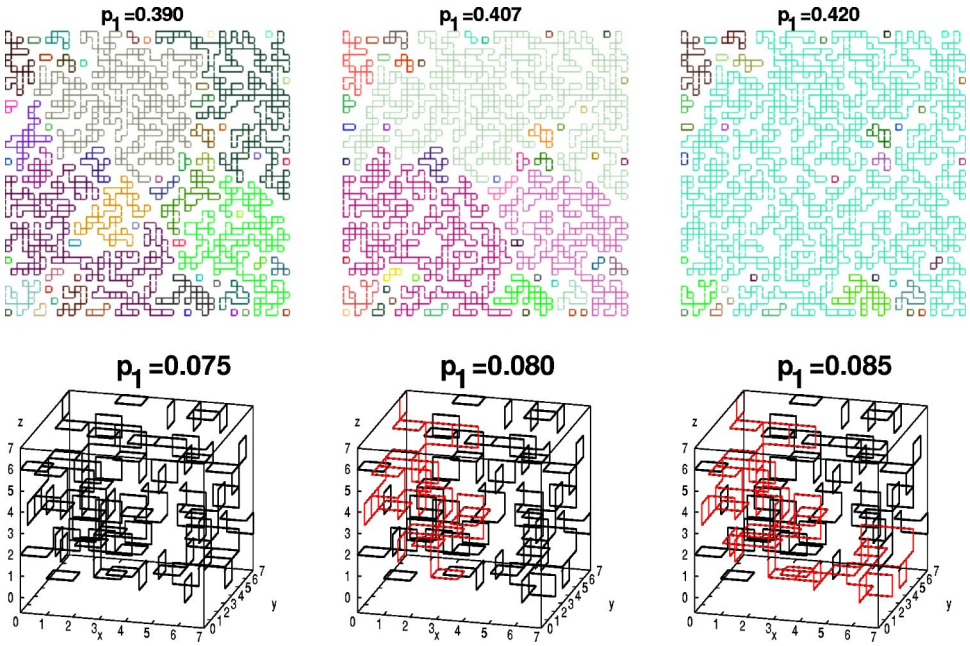

FIG. 2. FSS for the loop Hamiltonian (LH) model in 2D (top) and 3D (bottom). Plot of the percolation probability P^{perc} (left) and of the probability P_∞ for a bond belonging to a percolating loop (middle). The inset shows the raw data. (Right) Plot of the average number n_m of loops of mass m per lattice bond at $\sigma_c=0.458$ in 2D and at $\sigma_c=0.3129$ in 3D, respectively.

since they represent magnetic vortex lines that are divergence free. The real valued quenched random variables $b_i \in [-2\sigma, 2\sigma]$ are derived from the lattice curl of a random vector potential ($\sigma \geqslant 0$ being the strength of the disorder). The 3D vector $\mathbf{r}_i$ denotes the spatial positions of bond i in the lattice and the sum runs over all bond pairs of the lattice (not only nearest neighbors). The lattice propagator $G_\lambda(\mathbf{R})$ has the asymptotic form $G_\lambda(\mathbf{R}) \propto \exp(-|\mathbf{R}|/\lambda)/|\mathbf{R}|$, where λ is the screening length. In the strong screening limit $\lambda \to 0$ only the on-site repulsion survives [15] and gets

$$H_{\mathrm{VG}}^{\lambda \to 0} = \sum_i (n_i - b_i)^2, \tag{6}$$

which is the LH (3) in 3D that we intend to study here.

III. RESULTS

We use a *depth-first search* algorithm known from combinatorial optimization [14] to identify the connected loops. The number of realizations we used to get statistically averaged data varied from 500 for the largest system size to 20 000 for the smallest system size. In the following the error bars of our data are determined from the standard deviation. Their values are smaller than the symbol size in the figures and are therefore omitted. The critical exponents as well as the critical parameters have been chosen so that a good data collapse for a restricted set of our data is obtained. In the case of the finite size scaling a restricted set of data omits data, which are presumably outside the asymptotic scaling regime, namely, data with values far from the critical point and data for small system sizes L. To quantify the ''goodness'' of these fits, we used an appropriate cost function S [17], whose minimum value should be close to unity when the fit is statistically acceptable. For example, from the analysis of the order parameter P_∞ of the LH model, see Fig. 2, we achieved $S(\sigma_c, 1/\nu, \beta/\nu) \approx 1.33$ in 2D and 1.25 in 3D. In the case of the log-log graph we restricted to data with $m > 30$ for the LP model and $m > 10$ for the LH model independent of L. The upper boundary of the cluster mass m was chosen depending on L and the dimension d, in detail for the largest L: $m < 2500$ for the LP model and $m < 500$ in 2D and $m < 150$ in 3D for the LH model. The error bars for the exponents from the log-log plot were determined by a least square fit.

Figures 3 and 4 depict three typical loop configurations of the LP and LH models around the critical threshold, respectively, which clearly indicates a percolation phase transition for both models.

A. Loop percolation (LP) model

First, we study the LP model and consider the probability P^{perc} that a loop percolates the system. Since we assume to have only one typical length scale, which diverges at the critical point like $\xi \sim |p_1 - p_{1c}|^{-\nu}$, in a finite system P^{perc} is expected to scale like

$$P^{perc}(L) \sim \overline{P}[(p_1 - p_{1c}) L^{1/\nu}]. \tag{7}$$

Thus, $P^{perc}(L)$ is independent of L at p_{1c} and the data curves should intersect for different system sizes L. From our raw data in the inset of Fig. 5 (left) we locate the critical point $p_{1c} = 0.4070 \pm 0.0005$ in 2D and $p_{1c} = 0.0793 \pm 0.0004$ in 3D, respectively. We plot the scaling assumption (7) in Fig. 5 (left) and estimate the inverse correlation length exponent $1/\nu = 0.75 \pm 0.03$ in 2D and $1/\nu = 1.143 \pm 0.090$ in 3D from the best data collapse at fixed p_{1c}.

To get a second critical exponent we consider the probability P_∞ that a bond belongs to the percolating loop, i.e., the order parameter, which is expected to obey

$$P_\infty(L) \sim L^{-\beta/\nu} \overline{P}[(p_1 - p_{1c}) L^{1/\nu}]. \tag{8}$$

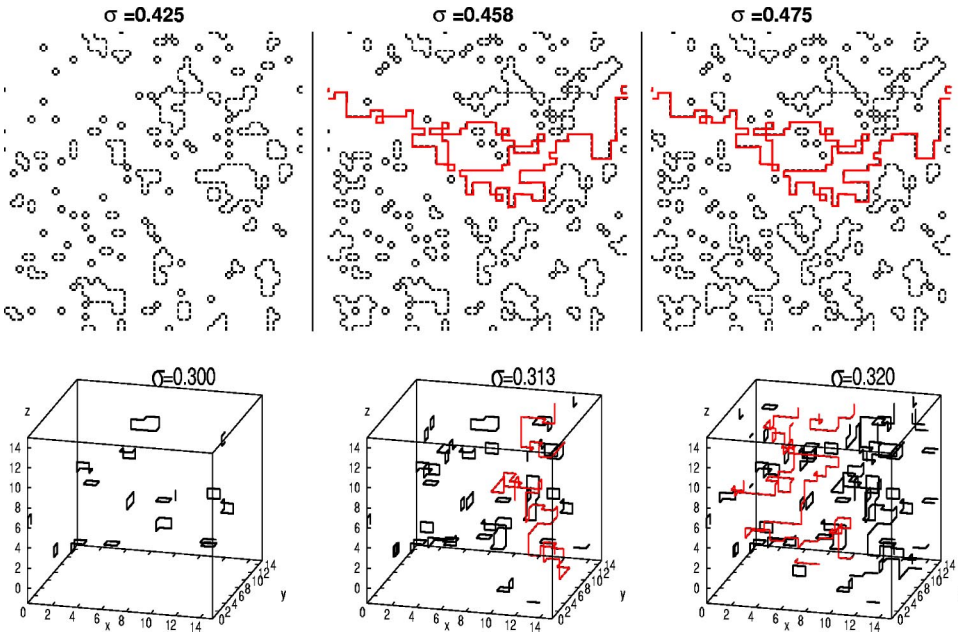

FIG. 3. Typical loop configurations of the LP model around the critical point $p_{1c} \approx 0.41$ in 2D (top) for $L=50$ and $p_{1c} \approx 0.08$ in 3D (bottom) for $L=8$. In 2D the different loops are marked by different gray scales (colors), whereas in 3D all loops are black except for the percolating loop, which is marked by light gray (red).

Figure 5 (middle) shows the raw data (inset) and the plot of the scaling law (8) with $\beta/\nu = 0.104 \pm 0.020$ in 2D and $\beta/\nu = 0.49 \pm 0.02$ in 3D, so as to achieve the best data collapse. From the ν above we determine β shown in Table I.

At the critical point p_{c1} the average number n_m of finite loops of mass m per lattice bond scales like

$$n_m(L, p_1 = p_{1c}) \sim m^{-\tau}, \tag{9}$$

where τ is the Fisher exponent [10,18]. Since we assume the usual scaling relations of conventional percolation to be valid [10], we also expect a combination of them to be valid, i.e., the hyperscaling relation

$$\tau = \frac{2 - \beta/(d\nu)}{1 - \beta/(d\nu)}, \tag{10}$$

where d is the spatial dimension. From the fit of the data of

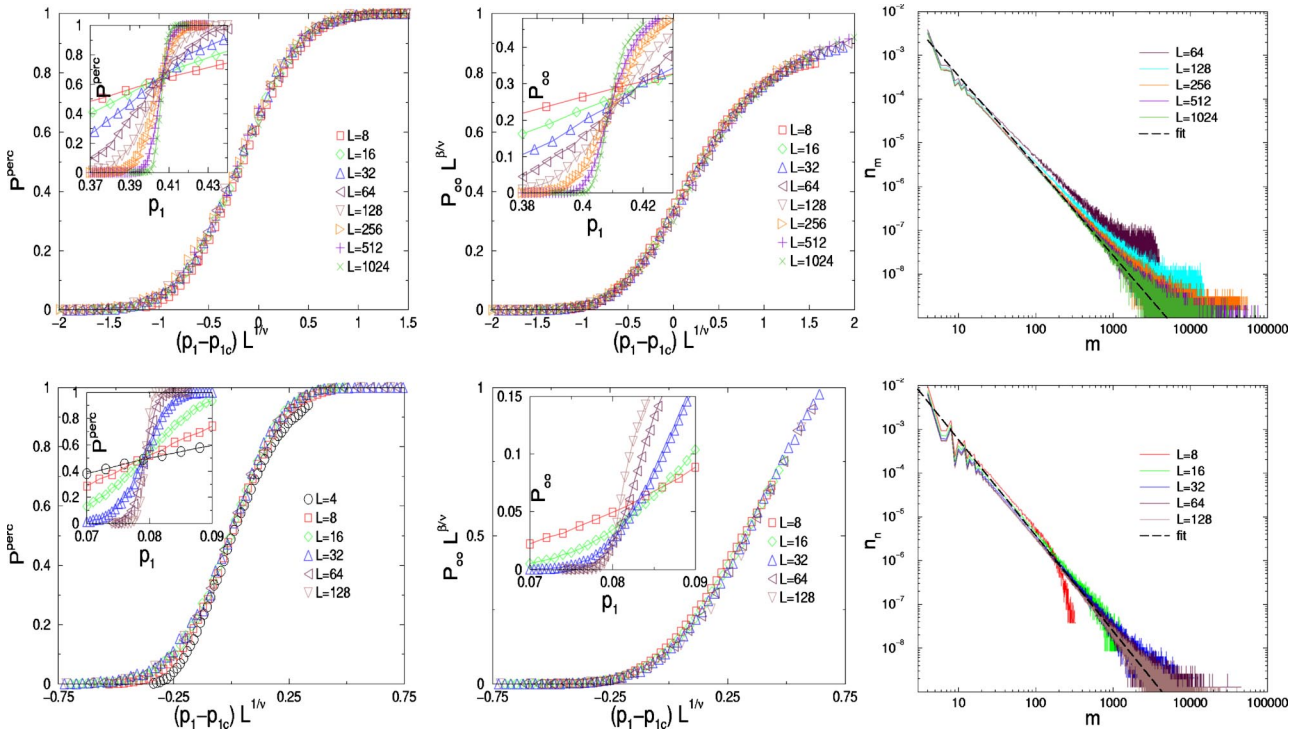

FIG. 4. Typical loop configurations of the loop Hamiltonian (LH) model in the ground state ($T=0$) around the critical point $\sigma_c \approx 0.46$ in 2D (top) for $L=50$ and $\sigma_c \approx 0.31$ in 3D (bottom) for $L=16$. In 2D and 3D all loops are black except for the percolating loop, which is marked by light gray (red).

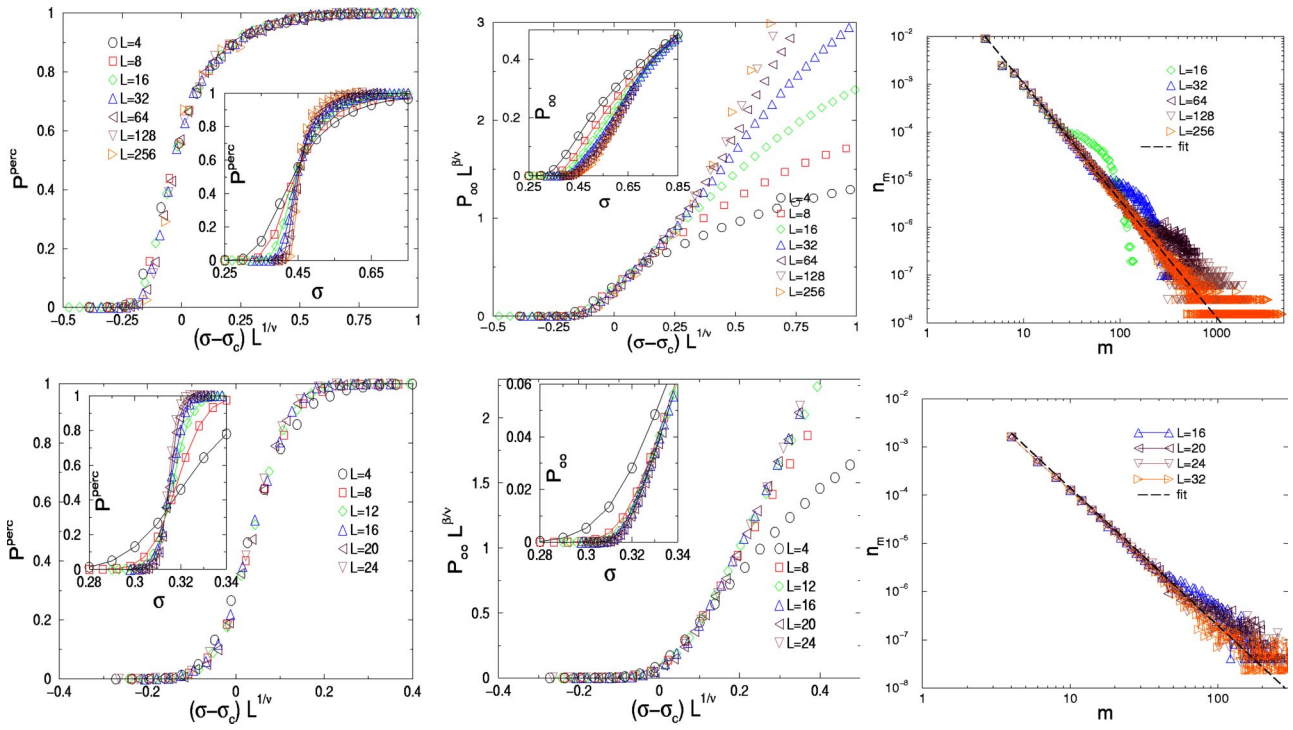

FIG. 5. Finite-size scaling (FSS) for the LP model in 2D (top) and 3D (bottom): plot of the percolation probability P^{perc} (left) and of the probability P_∞ for a bond belonging to a percolating loop (middle). The inset shows the raw data. (Right) Plot of the average number n_m of loops of mass m per lattice bond at $p_{1c}=0.407$ in 2D and at $p_{1c}=0.0793$ in 3D, respectively.

$n_m(L)$ at p_{c1} in Fig. 5 (right) we get τ depicted in Table I. This is consistent with the value obtained by putting the above ν and β into Eq. (10), i.e., $\tau=2.05\pm0.05$ in 2D and $\tau=2.20\pm0.06$ in 3D.

To determine the critical probability p_c that a bond is occupied, we calculate

$$p_c(L)=\sum_{m=4}^{m_L} m n_m(L;p_1=p_{1c}), \tag{11}$$

where m_L is the largest finite loop. We plot $p_c(L)$ versus $1/L$ as depicted in Fig. 6 and extract p_c from the limit $L\to\infty$.

TABLE I. Comparison of the critical thresholds and critical exponents for conventional bond percolation, the loop percolation (LP) model, and the loop Hamiltonian (LH) model.

		Conventional percolation [10]	Conventional bond percolation [22]	LH	LP	LP with singly occupied bonds
2D	p_c	0.5927460[a] and 1/2[b]	0.5000±0.0004	0.189±0.005	0.650±0.005	0.570±0.005
	p_{1c}				0.4070±0.0005	0.5485±0.0005
	σ_c			0.458±0.001		
	$P^{perc}(p_c)$		0.70±0.02	0.59±0.02	0.64±0.02	0.67±0.02
	ν	$4/3=1.\overline{3}$	1.33±0.05	3.33±0.30	1.33±0.05	1.33±0.04
	β	$5/36=0.13\overline{8}$	0.139±0.030	1.80±0.35	0.138±0.027	0.139±0.007
	τ			2.45±0.05	2.05±0.10	
3D	p_c	0.31161[a] and 0.248814[b]	0.2489±0.0002	0.0198±0.0005	0.282±0.005	0.267±0.005
	p_{1c}				0.0793±0.0004	0.0992±0.0005
	σ_c			0.3129±0.0005		
	$P^{perc}(p_c)$		0.63±0.02	0.34±0.02	0.53±0.02	0.54±0.02
	ν	0.875	0.875±0.070	1.05±0.05	0.875±0.070	0.875±0.070
	β	0.417	0.43±0.04	1.4±0.1	0.43±0.04	0.42±0.04
	τ			2.85±0.05	2.19±0.05	

[a]Conventional site percolation.
[b]Conventional bond percolation.

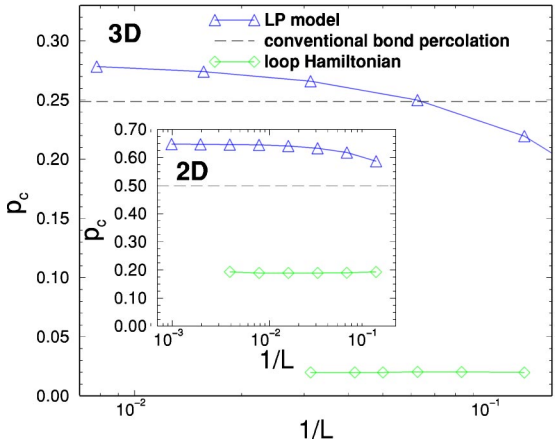

FIG. 6. Plot of the critical probability $p_c(L)$ vs inverse system size $1/L$ in 2D and in 3D for the conventional bond percolation model, the LP model, and the loop Hamiltonian (LH) model.

In addition to the results presented so far, we found that the mean number N^{perc} of percolating loops per sample in the finite system can be described by a smeared step function with an upper boundary $N^{perc}=1$, as known from conventional percolation [10]. When we define the mass m_i of an occupied bond i to be $m_i=1$ even for $|n_i|>1$, the critical scaling behavior remains unchanged and the critical probability becomes $p_c=0.565\pm0.005$ in 2D and $p_c=0.266\pm0.005$ in 3D, respectively. We also studied the case where the algorithm detects the loops along oriented paths, and found the same results, as expected from what we said above.

B. Loop Hamiltonian (LH) model

For loop Hamiltonian (3) we perform analogous data analysis. From the intersection of the L-dependent curves of $P^{perc}(L)$ in the inset of Fig. 2 (left) we locate the critical disorder strength at $\sigma_c=0.458\pm0.001$ in 2D and $\sigma_c=0.3129\pm0.0005$ in 3D, respectively. From the finite-size scaling behavior of the percolation probability P^{perc} [similar to Eq. (7)] we get $1/\nu=0.30\pm0.05$ in 2D and $1/\nu=0.95\pm0.05$ in 3D. The resulting exponent ν are given in Table I. In 2D we find a value $\nu=3.3\pm0.3$, which is rather large.

Figure 2 (middle) shows the plot of the raw data of P_∞ (inset) and its scaling law similar to Eq. (8) with $\beta/\nu=0.55\pm0.05$ in $2d$ and $\beta/\nu=1.30\pm0.05$ in 3D. From the ν above we determine β in Table I.

In Fig. 2 (right) we plot the loop distribution $n_m(L)$ vs the mass m at the critical point σ_c and determine τ by a power-law fit, which gives the values shown in Table I. From ν and β above we get via the hyperscaling relation (10) the Fisher exponent $\tau=2.38\pm0.17$ in 2D and $\tau=2.76\pm0.26$ in 3D, which are consistent with the values from the power-law fit within the error bars.

In Fig. 7 we plot the mean number N^{perc} of percolating loops per sample. The different curves of $N^{perc}(L)$ intersect at the same critical point σ_c found for P^{perc} above. Similar to the scaling law of $N^{perc}_{conv.}(L)$ in conventional percolation [10], we expect $N^{perc}(L)$ to obey

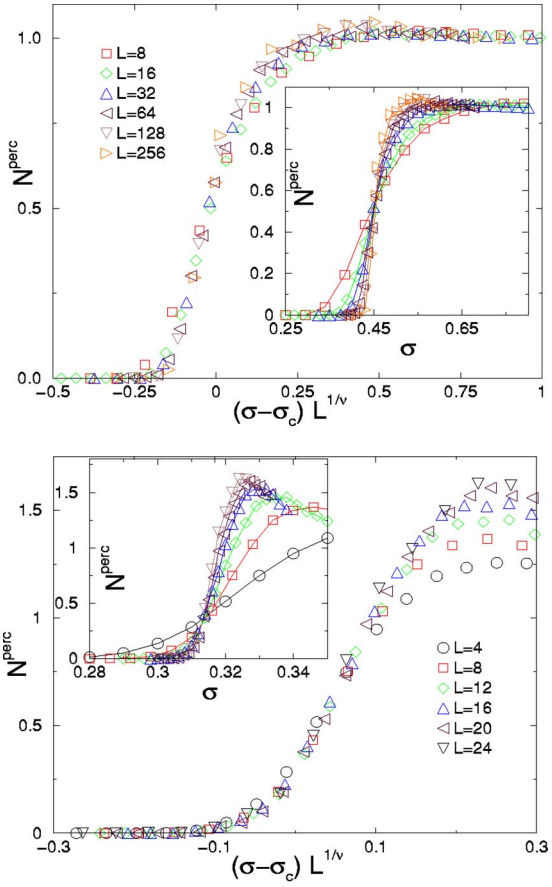

FIG. 7. Plot of the mean number N^{perc} of percolating loops for the loop Hamiltonian (LH) model in 2D (top) and 3D (bottom).

$$N^{perc}(L)\sim\overline{N}[(\sigma-\sigma_c)L^{1/\nu}], \tag{12}$$

and estimate the same ν as above from the best data collapse, see Fig. 7.

The mean number N^{perc} of percolating loops per sample can become larger than one slightly above the critical point σ_c in contrast to conventional percolation, where only one percolating cluster exists for $p>p_c$. The appearance of several percolating loops can possibly be related to the fact that the loop density in the LH model at σ_c is much smaller than in the LP model, as can be seen from comparison of typical loop configurations (cf. Figs. 3 and 4). Moreover, the maximum of $N^{perc}(L)$ seems to increase with increasing L. From our data we could not determine the behavior of the maximum of $N^{perc}(L)$ in the thermodynamic limit $L\to\infty$, in particular whether it converges to a constant or diverges. We also checked a L-dependent power-law behavior of $N^{perc}(L)$ similar to Eq. (8) with a new critical exponent x (instead of β) and found $x/\nu=0.01\pm0.01$ in 2D and $x/\nu=0.15\pm0.02$ in 3D, i.e., x close to zero.

Finally, we calculate the probability $p_c(L)$ that a bond is occupied [analogous to Eq. (11)] for different L at the critical point σ_c as shown in Fig. 6 and extract p_c as the average value, see Table I.

In all considered ground state configurations of loop Hamiltonian (3) we found a bond to be empty or singly

occupied only. Due to this observation we also investigated—besides the study presented this paper—a modified LP model, in which a plaquette is allowed to be occupied with p_1 if and only if the amount of the resulting flow $\mathbf{n}$ is $|n_i| \leqslant 1$. Here, the algorithm checked each plaquette to be occupied or not in positional order. Note that this occupation process depends on the algorithmic order of occupying plaquettes in the system. Again, we found the same critical exponents as known from conventional percolation, but a different critical probability p_{1c}.

We also studied the two-dimensional LH model with a different probability distribution function $P(b_i)$, where b_i is given by a sum of two uniformly distributed random numbers out of $[0,2\sigma]$. This corresponds to the SOS model on a disordered substrate, which has been studied [9,12] only at $\sigma = 1/2$ yet. For this probability distribution function we get the same critical exponents as found above, but with a different critical point at $\sigma_c = 0.395 \pm 0.005$, i.e., $p_c = 0.34 \pm 0.02$. This implies that our study is relevant to describe a disorder-driven flat–to–super-rough phase transition, not studied in literature yet.

Closely related to the SOS model is the two-dimensional model of a random elastic medium with contour loops, for which Zeng *et al.* found [13] the geometrical exponents $\beta/\nu = d - d_f = 0.54 \pm 0.01$ and $\tau = 2.32 \pm 0.01$ at $\sigma = 1/2$. These exponents agree with the critical $\beta/\nu = 0.55 \pm 0.05$ and $\tau = 2.38 \pm 0.17$ we found here at $\sigma_c \approx 0.458$.

IV. SUMMARY

We studied two loop percolation models, numerically: in the LP model the loop configuration resulted from an uncorrelated unbiased random occupation of elementary directed plaquettes, while in the LH model the loop configuration appeared according to the Boltzmann weight of a particular microscopic model at $T = 0$, i.e., from an optimization constraint (1) of a Hamiltonian (3). Our results are summarized in Table I.

We found that in 2D and 3D the LP model belongs to the universality class of the conventional (bond or site) percolation [10]. A plausible explanation for this observation is the following: We map an occupied (empty) plaquette onto an occupied (empty) site on an appropriate lattice. Figure 8 illustrates the mapping in 2d: the two loops on a square lattice of system size L, Fig. 8 (left), are mapped onto two clusters consisting of two and four occupied sites on a (dual) square lattice of size $L-1$, Fig. 8 (right). The resulting clusters of sites are clusters of finite extended objects such as k-mers in Ref. [19], which show the same universal behavior at the percolation transition as conventional site percolation [10]. Also we found that the nontrivial orientation of the loops in the LP model is irrelevant for the universality class. We expect that this also holds for higher spatial dimensions d with the same critical dimension $d_c = 6$ as for conventional percolation [10,20].

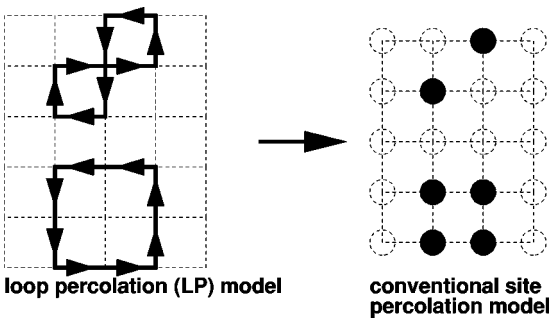

FIG. 8. Schematic mapping of the loops in the LP model (left) onto sites (filled circles) in the conventional site percolation model with next nearest neighbors (right; see text).

For the LH model, Eq. (3), we found evidence for an unconventional universality class of percolation in 2D and 3D; the exponents are listed in Table I. In 2D, we obtained a rather large correlation length exponent $\nu = 3.3 \pm 0.3$, which possibly indicates an infinite critical exponent for $L \to \infty$ known from the Kosterlitz-Touless (KT) phase transition [21]. On the other hand, since our Hamiltonian (3) has no XY, a KT transition can be ruled out. Indeed, from applying a KT form of finite-size scaling to our data, we could not find any acceptable data collapse.

It would be interesting to study the universal behavior of the pure (i.e., $\sigma = 0$) LH model (3) for finite temperatures T. In 3D, such a thermal-driven loop percolation phase transition has been studied [5] for a different model.

ACKNOWLEDGMENTS

We thank Jae Dong Noh for fruitful discussions and stimulating ideas. This work was supported financially by the Deutsche Forschungsgemeinschaft (DFG).

[1] G.A. Williams, Phys. Rev. Lett. **59**, 1926 (1987), and references cited therein.
[2] A.M.J. Schakel, Phys. Rev. E **63**, 026115 (2001).
[3] G.A. Williams, Phys. Rev. Lett. **82**, 1201 (1999), and references cited therein.
[4] Karl Strobl and Mark Hindmarsh, Phys. Rev. E **55**, 1120 (1997).
[5] A.K. Nguyen and A. Sudbø, Phys. Rev. B **58**, 2802 (1998).
[6] F.O. Pfeiffer and H. Rieger, J. Phys.: Condens. Matter **14**, 2361 (2002).
[7] S.T. Chui and J.D. Weeks, Phys. Rev. B **14**, 4987 (1976).
[8] J. Toner, Phys. Rev. Lett. **66**, 679 (1991).
[9] H. Rieger and U. Blasum, Phys. Rev. B **55**, 7394 (1997).
[10] D. Stauffer, *Introduction to Percolation Theory* (Taylor & Francis, London, 1985); A. Bunde and S. Havlin, *Fractals and Disordered Systems*, 2nd ed. (Springer, New York, 1996).
[11] J. Kisker and H. Rieger, Phys. Rev. B **58**, R8873 (1998); F. Pfeiffer and H. Rieger, *ibid.* **60**, 6304 (1999).
[12] F.O. Pfeiffer and H. Rieger, J. Phys. A **13**, 2489 (2000).
[13] C. Zeng, J. Kondev, D. McNamara, and A.A. Middleton, Phys. Rev. Lett. **80**, 109 (1998).
[14] A. Hartmann and H. Rieger, *Optimization Algorithms in Phys-*

ics (Wiley-VCH, Berlin, 2002).
[15] H.S. Bokil and A.P. Young, Phys. Rev. Lett. **74**, 3021 (1995).
[16] J.M. Kosterlitz and M.V. Simkin, Phys. Rev. Lett. **79**, 1098 (1997).
[17] N. Kawashima and N. Ito, J. Phys. Soc. Jpn. **62**, 435 (1993).
[18] M.E. Fisher, Physics **3**, 255 (1967).
[19] Y. Leroyer and E. Pommiers, Phys. Rev. B **50**, 2795 (1994).
[20] J. Cardy, *Scaling and Renormalization in Statistical Physics* (Cambridge University Press, Cambridge, 1997).
[21] J.M. Kosterlitz and D.J. Touless, J. Phys. C **6**, 1181 (1973).
[22] We reproduced the results of conventional bond percolation for comparison, where we used parameters (i.e., number of samples and system sizes) similar to the study of the LP model.